iScience

CellPress
OPEN ACCESS

Article

HBD-2 binds SARS-CoV-2 RBD and blocks viral entry: Strategy to combat COVID-19

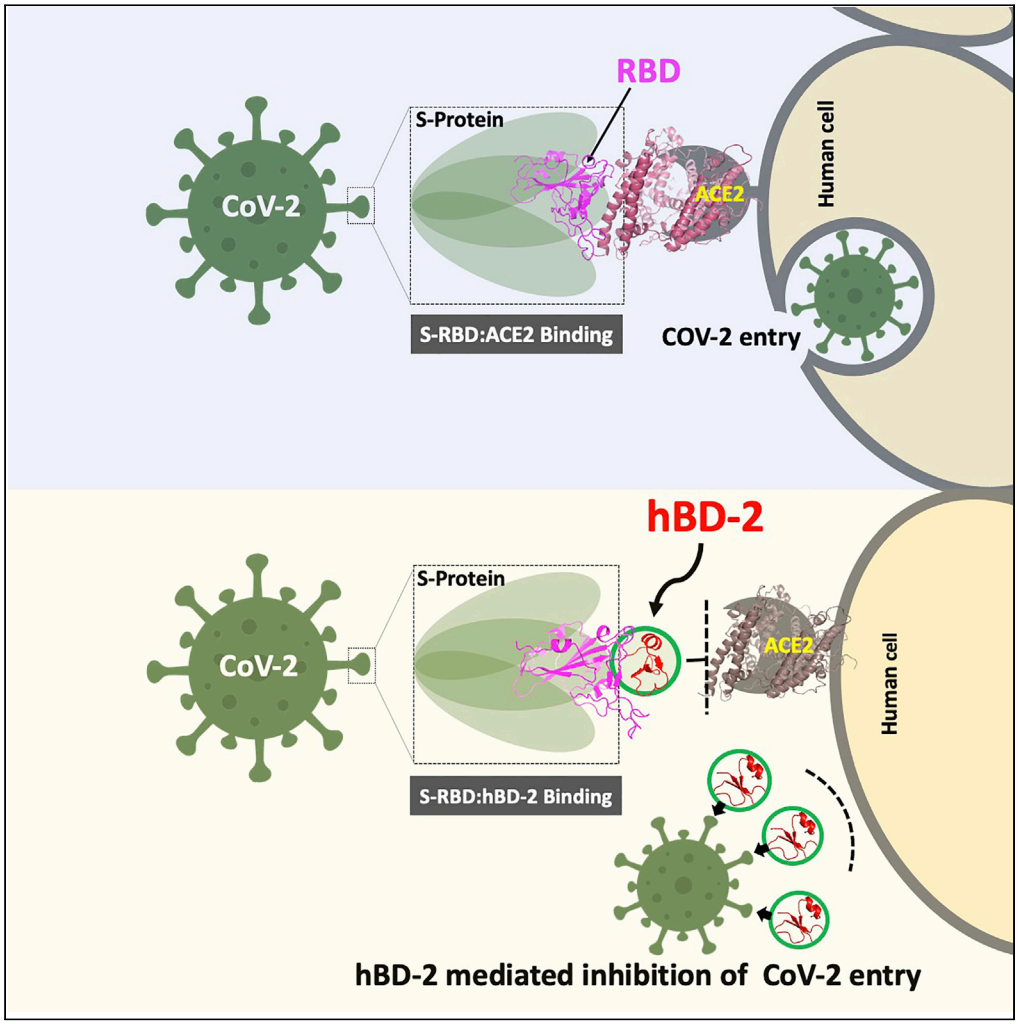

Liqun Zhang, Santosh K. Ghosh, Shrikanth C. Basavarajappa, ..., Parameswaran Ramakrishnan, Matthias Buck, Aaron Weinberg

pxr150@case.edu (P.R.)
mxb150@case.edu (M.B.)
axw47@case.edu (A.W.)

Highlights

HBD-2 binds spike-RBD at the ACE2 interaction site in silico

Biophysical and biological assays confirm hBD-2 binding to spike-RBD

HBD-2 blocks spike-RBD:ACE2 binding

HBD-2 prevents CoV-2/spike pseudovirions from infecting ACE2-expressing human cells

Zhang et al., iScience *25*, 103856
March 18, 2022 © 2022 The Author(s).
https://doi.org/10.1016/j.isci.2022.103856

iScience

CellPress
OPEN ACCESS

Article

HBD-2 binds SARS-CoV-2 RBD and blocks viral entry: Strategy to combat COVID-19

Liqun Zhang,[1,5] Santosh K. Ghosh,[2,5] Shrikanth C. Basavarajappa,[3,5] Yinghua Chen,[4] Pravesh Shrestha,[4] Jackson Penfield,[1] Ann Brewer,[1] Parameswaran Ramakrishnan,[3,*] Matthias Buck,[4,*] and Aaron Weinberg[2,6,*]

SUMMARY

New approaches to complement vaccination are needed to combat the spread of SARS-CoV-2 and stop COVID-19-related deaths and medical complications. Human beta defensin 2 (hBD-2) is a naturally occurring epithelial cell-derived host defense peptide that has anti-viral properties. Our comprehensive *in-silico* studies demonstrate that hBD-2 binds the site on the CoV-2-RBD that docks with the ACE2 receptor. Biophysical measurements confirm that hBD-2 indeed binds to the CoV-2-receptor-binding domain (RBD) ($K_D \sim 2\mu M$ by surface plasmon resonance), preventing it from binding to ACE2-expressing cells. Importantly, hBD-2 shows specificity by blocking CoV-2/spike pseudoviral infection, but not VSVG-mediated infection, of ACE2-expressing human cells with an IC_{50} of $2.8 \pm 0.4\ \mu M$. These promising findings offer opportunities to develop hBD-2 and/or its derivatives and mimetics to safely and effectively use as agents to prevent SARS-CoV-2 infection.

INTRODUCTION

SARS-CoV-2 (CoV-2) continues to impact worldwide health, having claimed over four million lives as of August 2021 (worldometers.info/coronavirus/). The discovery of new approaches to complement vaccinations and impede the virus' relentless spread remains an urgent challenge. CoV-2 expresses the spike (S) protein (Siu et al., 2008; Yoshimoto, 2020), which is responsible for binding to the receptor ACE 2 (ACE2), followed by fusion of the viral and cellular membranes. To engage ACE2, the receptor-binding domain (RBD) of the S protein undergoes hinge-like conformational movements that transiently hide or expose its determinants for receptor binding (Wrapp et al., 2020). Becausethis is a critical initial event in the infection cascade, the RBD is a key target for therapeutic strategies (Tai et al., 2020). The high degree of dynamics of the RBD:ACE2 complex (Brielle et al., 2020; Ghorbani et al., 2020; Spinello et al., 2020) suggests that binding of small flexible peptides may inhibit spike protein:host cell receptor interactions, which can be interrogated by computational modeling and simulations most suitable for exploring these interactions (Amaro and Mulholland, 2020).

Nature's own antimicrobial peptides (AMPs) have been proposed as multifunctional defenses that participate in the elimination of pathogenic microorganisms, including bacteria, fungi, and viruses (Mookherjee et al., 2020). Exhibiting antimicrobial and immunomodulatory properties, AMPs have been intensively studied as alternatives and/or adjuncts to antibiotics in bacterial infections and have also gained substantial attention as anti-viral agents (Mulder et al., 2013). Human beta defensins (hBDs), the major AMP group expressed in mucosal epithelium, provide a first line of defense against various infectious pathogens, including enveloped viruses (Leikina et al., 2005; Quiñones-Mateu et al., 2003; Ryan et al., 2011). HBD-2 is expressed throughout the respiratory epithelium from the oral cavity to the lungs, and plays an important role in defense against respiratory infections (Mookherjee et al., 2020). It is an amphipathic, beta-sheeted, cationic (+6 charge) molecule of 41 amino acids, and is stabilized by three intramolecular disulfide bonds that protect it from degradation by proteases (Sawai et al., 2001).

In the present study, we examined the ability of hBD-2 to act as a blocking agent against CoV-2. Through extensive *in silico* docking and molecular dynamics simulation analyses we discovered that hBD-2 binds to the receptor-binding motif (RBM) of the RBD of CoV-2 that associates with the ACE2 receptor. Biophysical and biochemical studies, respectively, confirm that hBD-2 binds the RBD and also prevents it from binding ACE2. By utilizing a CoV-2 spike-pseudotyped luciferase assay platform, we revealed that hBD-2 effectively blocks CoV-2 spike-expressing pseudovirions from entering ACE2-expressing human cells. Harnessing the

[1]Chemical Engineering, Tennessee Technological University, Cookeville, TN 38505, USA

[2]Biological Sciences, School of Dental Medicine, Case Western Reserve University, Cleveland, OH 44106, USA

[3]Department of Pathology, School of Medicine, Case Western Reserve University, Cleveland, OH 44106, USA

[4]Department of Physiology and Biophysics, School of Medicine, Case Western Reserve University, Cleveland, OH 44106, USA

[5]These authors contributed equally

[6]Lead contact

*Correspondence: pxr150@case.edu (P.R.), mxb150@case.edu (M.B.), axw47@case.edu (A.W.)

https://doi.org/10.1016/j.isci.2022.103856

This is an open access article under the CC BY-NC-ND license (http://creativecommons.org/licenses/by-nc-nd/4.0/).

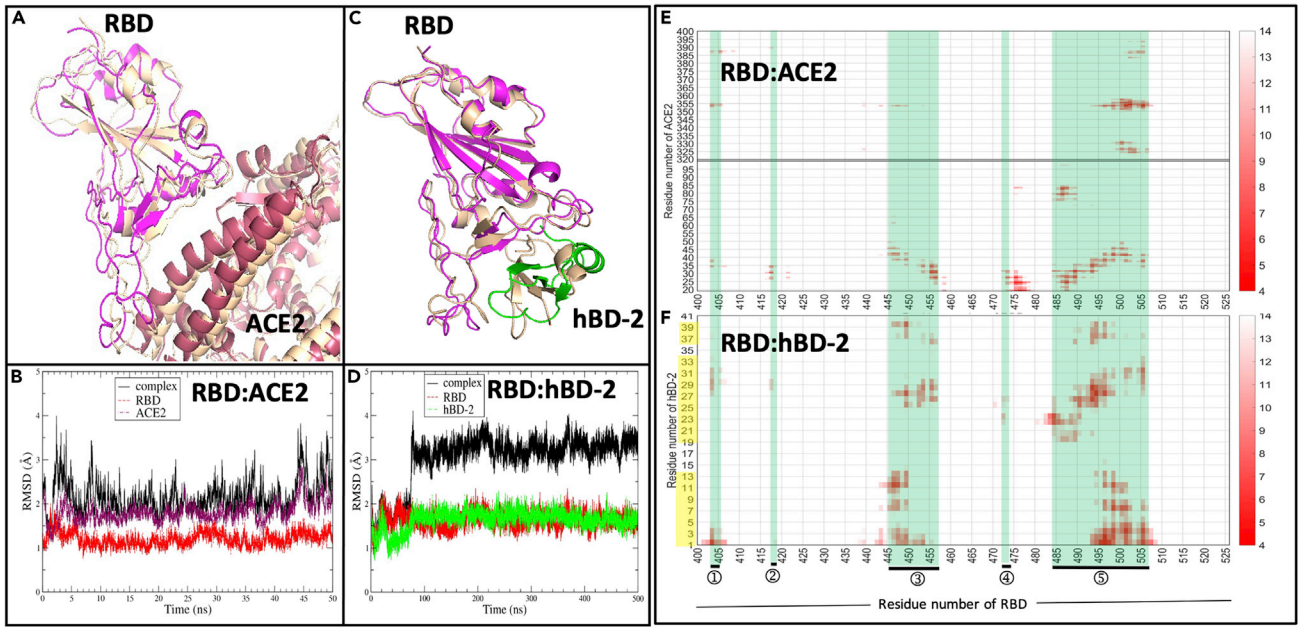

Figure 1. Molecular dynamics simulations of RBD:ACE2 and RBD:hBD-2 (monomer) show stable protein complex

(A) Comparison of the initial structures (shown in sand-color) and last structure (shown in raspberry for ACE2 and magenta for RBD) after 50 ns all-atom MD simulation for the RBD from SARS-COV-2 spike protein in complex with ACE2.

(B) RMSD for RBD, ACE2, and RBD:ACE2 complex as a function of simulation time. The overall rms deviation (RMSD Ca) is ~1.2 Å, for ACE2, ~2.1 Å for the RBD and ~2.4 Å for the complex.

(C) Comparison of the initial (shown in sand-color) and last structures (shown in green for hBD-2 and magenta for RBD) after 500 ns all-atom MD simulations for the RBD:hBD2 complex.

(D) RMSD of RBD, hBD-2, and RBD:hBD-2 complex as function of simulation time.

(E and F) Distance map of inter-protein contacts in (E) the RBD:ACE2 complex and (F) in the RBD:hBD-2 complex with distances color coded by average proximity over the length of the simulations (see color scale in Å, right). Five regions of the RBD shaded in green are common regions for binding the two proteins; hBD-2 residues in contact with RBD are shaded yellow on y axis.

utility of naturally occurring AMPs, such as hBD-2, and their derived smaller peptides, could be a viable approach in developing novel CoV-2 therapeutics.

RESULTS

Interaction of SARS-CoV-2 RBD with ACE2 and hBD-2 using *in silico* docking and molecular dynamics simulations

A. *RBD:ACE2 complex*: We ran, as a reference, a 50-ns all-atom molecular dynamics (MD) simulation of the ACE2:RBD complex. The final structure is compared with the initial experimental structure (Lan et al., 2020) in Figure 1A. Only moderate deviations are seen in some of the loop regions and at the N- and C-termini of both proteins (Figure 1B). The solvent accessible surface area, buried between the RBD and ACE2 proteins in the complex, fluctuates only modestly (750–1000 $Å^2$ around an average of ~900 $Å^2$ over the last 25 ns of the trajectory), further indicating the overall stability of the complex in the simulations.

B. *RBD:hBD-2 (monomer)*: We carried out docking with CLUSPRO and HADDOCK (see STAR Methods) to explore the initial possible bound structures between the RBD and hBD-2. In the case of CLUSPRO, the entire proteins were assessed for possible interaction surfaces. The best predicted models involved the receptor-binding motif (RBM) of the RBD, and these structures were used as starting structures for all-atom MD and carried out for up to 500 ns. We also ran repeat simulations with different starting seeds (initial velocity assignments). All simulations are summarized in Table S1. By comparing the initial and final structures, and presenting the most stable trajectory (Figures 1C and D), we observed visually, and by RMSD, a slight rotation of hBD-2 relative to the initial structure at 75 ns. However, for the remaining 425 ns, hBD-2 stayed in the same location but made a range

of interactions. This observation is remarkable because it is becoming clear that many protein complexes with the moderate binding affinity of ACE2:RBD and hBD-2:RBD are considerably dynamic and that the initial association involves many encounter states, with a majority not even involving the final interfaces (e.g. Li and Buck, 2019). The persistency of the complex was also confirmed by the amount of surface area buried between the two proteins, fluctuating moderately around a value of 700 $\pm$ 150 Å^2. The value is smaller than that seen on binding to ACE2 (900 Å^2), indicating that less area is covered, consistent with the smaller size of hBD-2. The three repeat trajectories exhibited comparable interactions of hBD-2 with RBD (Figure S2).

A distance map, comparing residues which are on average closer than 5 Å in the RBD:ACE2 and RBD:hBD-2 complexes is shown in Figures 1E and 1F. For the RBD:ACE2, interaction residues 20 to 45, 75 to 85, as well as a short stretch of residues around 327, 355, and 387 on ACE2 bind with the RBD, whose binding interface ranges from residue 445 to 505. Some of the RBD residues are in loop regions, e.g., 404 and 417, which also come close to ACE2 over the course of the simulation. In total, five regions of the RBD (shaded in green) are involved. Remarkably, essentially all residues of the RBD, which contact ACE2 (either the same ones or their close neighbors), are also in contact with hBD-2 (Figure 1F; also shaded green). There are, however, some subtle shifts; i.e., RBD residues 475–478 make contact with ACE2 (shaded region 4; Figure 1E) but not with hBD-2, where these interactions may have shifted to residue 473. Also, a regional area of RBD residues 438–444 contacts hBD-2, an area not seen interacting with ACE2, possibly because it is less dynamic. These alternative interactions may provide a mechanistic entry for hBD-2 in replacing/competing away ACE2 from the spike trimer.

C. *Dynamics in the RBD:hBD-2 compared to the RBD:ACE2 complex:* The rms fluctuation (RMSF Ca) of each residue in the RBD and ACE2, both when they are in the complex and as differences between free and bound proteins are shown in Figure S2A and S2B, respectively. As expected, most regions at the RBD:ACE2 interaction interface become less flexible, while other changes, including increases in fluctuations are seen further away from the interface, consistent with the recent description of allostery in the spike protein (Gross et al., 2020). Upon complex formation, the RBD and ACE2 proteins form intermolecular hydrogen bonds (Figure S2C), which is one of the driving forces for their binding. Importantly, these bonds are highly dynamic with occupancy between 20% and 40% (Figure S1D). In total, seven of the 9 H-bonds of the RBD:ACE2 interface in the crystal structure (Lan et al., 2020) are populated with reasonable occupancy in the simulations. Similar behavior has been seen in other simulations (Ghorbani et al., 2020; Spinello et al., 2020) with the difference likely explained by solution vs. crystallization conditions. Water molecules were observed at the interface in other simulations and are likely bridging the interactions (Ali and Vijayan, 2020), also underscoring the dynamic nature of the interactions (see below).

The comparison of main-chain fluctuations in RBD:hBD-2, again between the bound and free states of the proteins, is shown in Figure 2A. Overall, the binding region becomes less flexible on the RBD in similar key regions which exhibited dampened dynamics by ACE2 binding, while on the side of hBD-2 a number of main-chain sites also see their fluctuations decreased (Figure 2B, showing results mapped to the final structure). Intermolecular hydrogen bonds (Figure 2C) are fewer, with an average 4 $\pm$ 1, compared to those bridging the RBD:ACE2 complex (Figure S2C). With exception of the Glu 484: Arg 23 hydrogen bond with a greater than 50% persistency (Figure 2D), the occupancy of other hydrogen bonds is reduced compared to the reference complex, suggesting that they are somewhat more dynamic (see discussion below) and are likely accompanied by indirect H-bond interactions with water molecules near or at the interface bridging the interactions.

D. *RBD:hBD-2 (dimer)*: Although the dimerization of hBD-2 by itself is modest (Hoover et al., 2000), it is possible that binding to the RBD stabilizes the dimeric form. We, therefore, also docked the hBD-2 dimer to the RBD and carried out simulations. Results are given in Figures S3A–S3D, suggesting that binding of an hBD-2 dimer is slightly stronger, H-bonds are more persistent, and that both units of the dimer make contact with the RBD.

E. *RBD:hBD-2-interaction energy calculation:* The average interaction energies, calculated with GBSA (see STAR Methods) have similar magnitudes and all are slightly negative (Figure S4). The average binding energy of the RBD:ACE2 is -45 ± 7 kcal/mol whereas average binding energy of RBD:hBD-2 (monomers) is -34 ± 8 kcal/mol (and is similar to that of the RBD:hBD-2 dimer). These estimates for

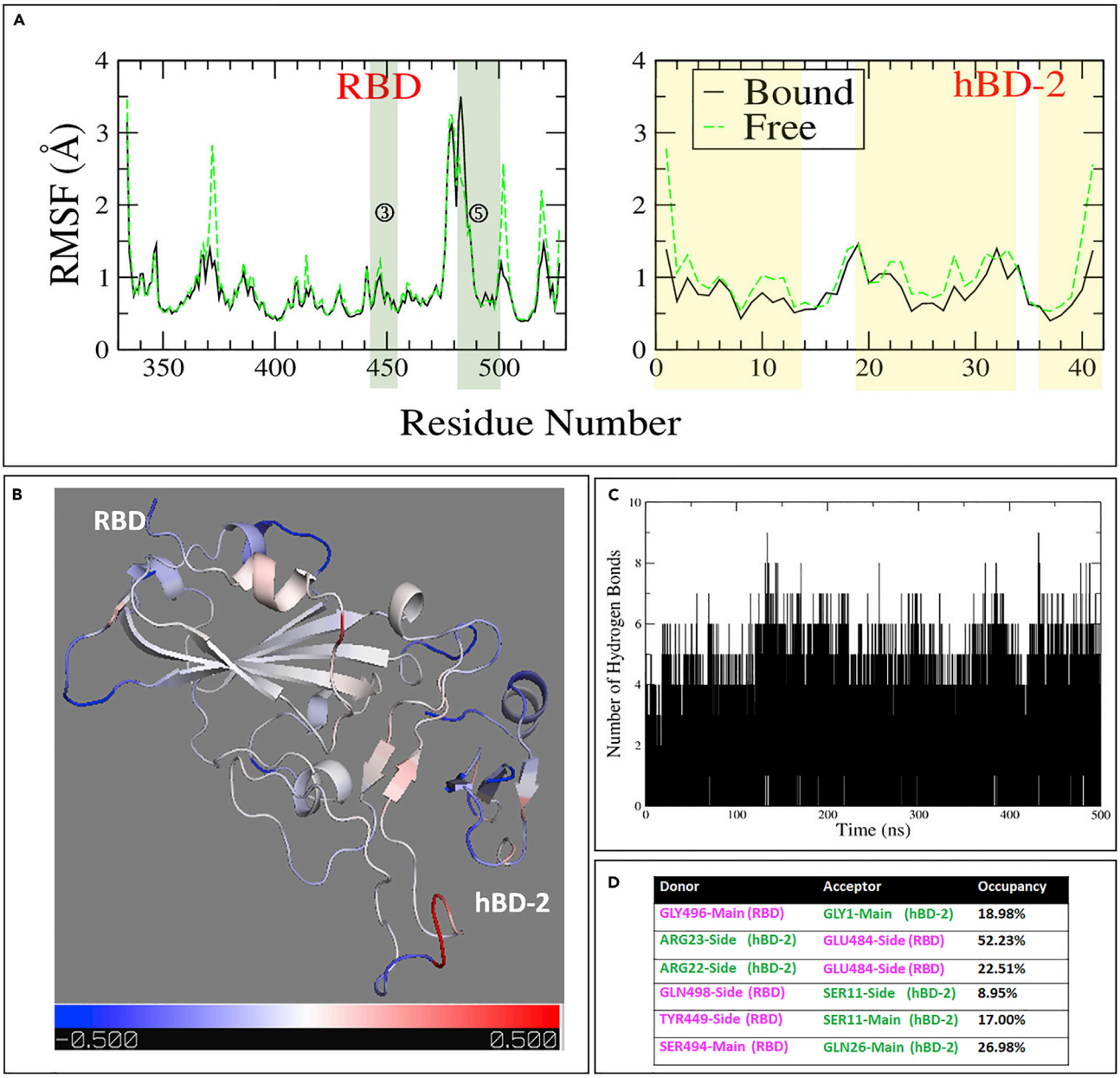

Donor	Acceptor	Occupancy
GLY496-Main (RBD)	GLY1-Main (hBD-2)	18.98%
ARG23-Side (hBD-2)	GLU484-Side (RBD)	52.23%
ARG22-Side (hBD-2)	GLU484-Side (RBD)	22.51%
GLN498-Side (RBD)	SER11-Side (hBD-2)	8.95%
TYR449-Side (RBD)	SER11-Main (hBD-2)	17.00%
SER494-Main (RBD)	GLN26-Main (hBD-2)	26.98%

Figure 2. The RBD and hBD-2 proteins retain considerable dynamics as a complex

(A) RMSF of RBD (left) and hBD-2 (right) in the complex over 500 ns in comparison with values for the unbound (free) proteins; the secondary structure of ACE2 and RBD are indicated (color shading as Figures 1E and 1F).

(B) Cartoon representation of the complex showing difference in RMSF between bound and free proteins. The data are mapped to the cartoon representation of the complex with color bar (bottom) indicating the range of −0.5 Å (in blue) to 0.5 Å (in red).

(C) Number of hydrogen bonds for the RBD bound to hBD-2 over the 500ns simulation.

(D) Table of most prominent h-bonds and their occupancy.

the free energy of binding have a greater negative value (suggesting stronger binding) than the experimental binding energy which is measured to be −10 kcal/mol to −12 kcal/mol. Nevertheless, our prediction is consistent with the reports of others (e.g. He et al., 2020), using the same computational method, who calculated a free energy for the RBD:ACE2 interaction of −50.4 kcal/mol. However, it is likely that the entropy change upon binding of the RBD to hBD-2 is more favorable, at least from a protein dynamics and solvation perspective, compared to that of RBD binding to ACE2. This is

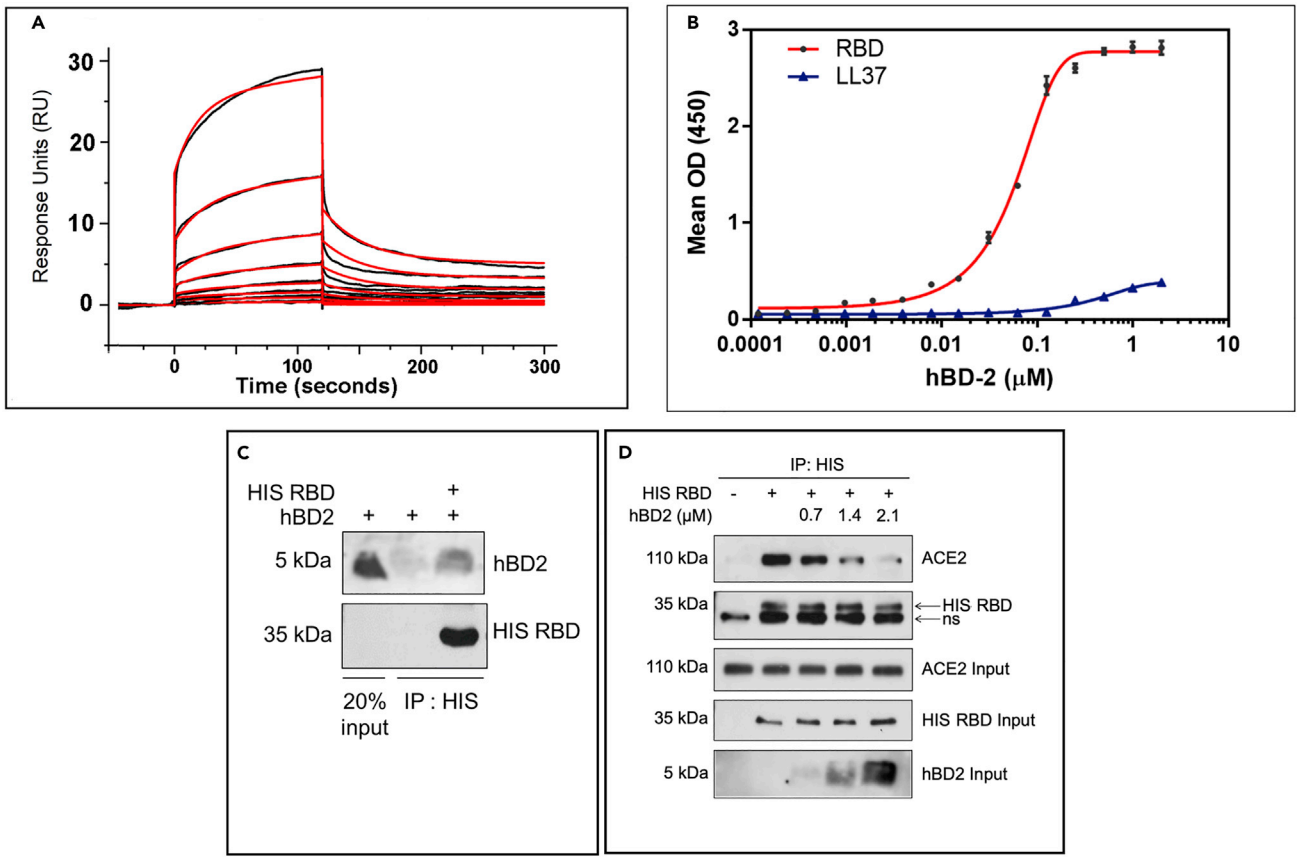

Figure 3. Biophysical and biological assays demonstrate that hBD-2 binds to RBD

(A) Concentration-dependent binding of recombinant hBD-2 (rhBD-2) to biotinylated recombinant RBD using surface plasmon resonance. The hBD-2 concentration ranged from 90 to 23,000 nM (see STAR Methods). Fitted data are from two experiments (the first experiment for SPR is shown giving a Kd of 2.8 μM).

(B) Functional ELISA assay showing that rhBD-2 specifically binds to immobilized rRBD. LL37 was used as a negative control.

(C) Recombinant His-RBD (0.19 μM) and hBD-2 (1.75 μM) were incubated as described in STAR Methods and precipitated with Ni-NTA beads to pull down His-tagged-RBD. Co-precipitation of hBD-2 was assessed by western blotting. Lane one shows 20% input of rhBD-2 and lane two shows Ni-NTA precipitation for background binding of rhBD-2 to the beads. Data are representative of three independent experiments. Control western blots showed modest background with hBD-2 alone.

(D) ACE2-expressing HEK 293T cells were incubated with HIS-RBD containing culture supernatant, with and without hBD-2 at 0.7–2.1 μM concentrations. Ni-NTA immunoprecipitation was performed to precipitate ACE2 bound to HIS-RBD and to assess the effect of hBD-2 addition on RBD:ACE2 binding. Data are representative of three independent experiments. ns indicate non-specific band.

because hBD-2 is more dynamic in the bound state, giving less of an entropy penalty upon binding. A caveat is that the surface buried is smaller between hBD-2 and the RBD than between ACE2 and the RBD and that in the latter complex there may be long-range dynamic allosteric changes.

Functional studies confirming binding of hBD-2 with the RBD

We used plasmon surface resonance (SPR) to measure binding of recombinant hBD-2 (rhBD-2) with recombinant RBD (rRBD) and determined an affinity of 1.8 ± 1.1 μM (Figure 3A). For measurements using microscale thermophoresis (MST), see Figure S5. We then followed up using a functional ELISA assay and found that rhBD-2 specifically bound to immobilized rRBD (Figure 3B). Incubating rhBD-2 (1.75 μM) with His-tagged rRBD (His-rRBD; 0.19 μM), followed by nickel bead immunoprecipitation and probing for hBD-2 in western blots, resulted in significant binding of hBD-2 to His-RBD (Figure 3C).

HBD-2 blocks the binding of RBD with ACE2

We utilized HEK 293T cells that overexpress the human ACE2 receptor in the assays and incubated these cells with HIS-RBD containing culture supernatant with and without rhBD-2. We immunoprecipitated RBD

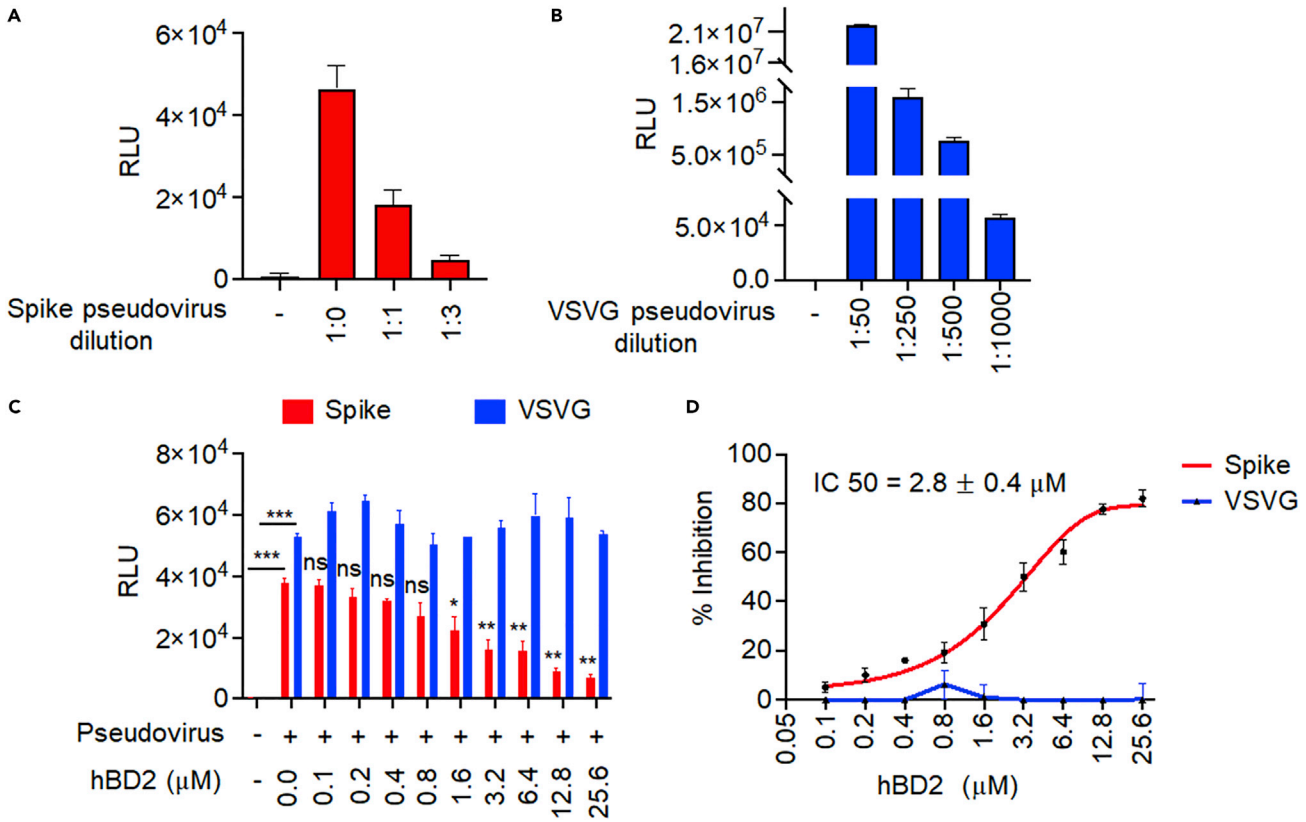

Figure 4. HBD-2 inhibits CoV-2 spike-pseudotyped viral entry into ACE2 293T cells

(A and B) Cells were incubated with CoV-2 Spike/VSVG-pseudotyped virus media at different dilutions and luciferase activity was measured at 48 h post infection (n = 2).

(C) Dose-response relationship of rhBD-2 against CoV-2 spike/VSVG-pseudotyped virus. Cells were co-infected with VSVG-pseudotyped (n = 4) or CoV-2 spike-pseudotyped (n = 4) virus along with varying amounts of rhBD-2 (0–25.6 μM) and luciferase activity was assessed.

(D) Percent inhibition of spike-viral entry by rhBD-2 was calculated from RLU values in (C); IC_{50} was calculated by plotting rhBD2 concentration (μM log) against % inhibition observed (n = 4). Values are Mean ± SEM ***p < 0.001, **p < 0.01, *p < 0.05, and ns (non-significant) against CoV-2 spike-pseudotyped virus alone treated group.

through the HIS-tag and examined the co-precipitation of ACE2. HIS-RBD effectively precipitated ACE2 and the addition of rhBD-2 competitively decreased RBD-ACE2 binding (Figure 3D).

HBD-2 specifically inhibits SARS-CoV-2 spike-mediated pseudoviral infection

A luciferase reporter expressing CoV-2 spike-dependent lentiviral system (Crawford et al., 2020) was used to study the competitive inhibitory effects of rhBD-2 on CoV-2 spike-mediated infection. To demonstrate that the inhibitory effect of hBD-2 is specific to spike-mediated infection, we used a vesicular stomatitis virus glycoprotein (VSVG)-pseudotyped virus as a control. Viruses pseudotyped with VSVG are pantropic, i.e., they can infect all cell types (Lever et al., 2004), and do not depend on ACE2 for entry. We infected ACE2-expressing HEK 293T cells using different dilutions of the luciferase-expressing spike or VSVG-pseudotyped virus as a control, to determine similar relative RLUs that correspond to a comparable MOI. We found that the infection of undiluted spike pseudotyped virus was similar to the infection obtained using a 1:1000 dilution of the VSVG pseudotyped virus (Figures 4A and 4B), which was used in the subsequent experiments. To study the hBD-2-mediated inhibition of viral entry, we co-infected cells with spike or VSVG-pseudotyped virus with varying amounts of rhBD-2. To better represent real-life infection, rhBD-2, spike pseudovirions and cells were incubated simultaneously, thereby preventing any advantage preincubation would have offered hBD-2. Additionally, preincubation of rhBD-2 with pseudovirions could have confounded results due to possible perturbation of viral membranes by the AMP. We found that rhBD-2 dose-dependently decreased entry of CoV-2 spike-mediated infection (Figure 4C; red bars) with the inhibitory concentration$_{50}$ (IC_{50}) of 2.8 ± 0.4 μM (Figure 4D; red line). rhBD-2 showed maximum inhibition of

spike-mediated pseudoviral infection by 80% at a concentration of 12.8 μM and plateaued thereafter (Figures 4C and 4D). Interestingly, addition of a range of rhBD-2 (0–25.6 μM) concentrations showed no inhibition of VSVG-pseudotyped virus infection (Figures 4C blue bars, 4D blue line), demonstrating the specificity of hBD-2 in inhibiting CoV-2 spike-mediated infection.

DISCUSSION

Beta defensins are localized to the mucosa of the oral cavity, nares, and upper airway (Diamond and Ryan, 2011; Ghosh et al., 2007; Khurshid et al., 2017; Lee et al., 2002; Mathews et al., 1999; Singh et al., 1998), sites deemed vulnerable to CoV-2 entry and initial infection. Indeed, hBD-2 has been shown to interrupt viral infection of various viruses, including coronaviruses (Kim et al., 2018). However, when a mucosal site becomes overwhelmed by a microbial threat, replenishing the AMP armamentarium locally after initial release takes multiple hours. Nasopharyngeal swab samples have revealed that patients infected with CoV-2 have lower mRNA levels of several defensins including hBD-2 (Idris et al., 2020). Thus, hBD-2 or their mimetics, if administered exogenously, could be a sound therapeutic strategy to protect the host at vulnerable mucosal sites without eliciting an immunological response.

We chose to investigate hBD-2's ability to block CoV-2 because of its innate role in protecting the oral cavity and the upper airway, and because its mouse ortholog has been shown to inhibit other coronaviruses (Zhao et al., 2016). The computer simulations showed remarkable stability of the RBD:hBD-2 complex even after 500 ns, with a clear overlap of binding sites when compared to the RBD:ACE2 complex. Complementary methods involving SPR, ELISA, and immunoprecipitation/western blotting independently verified that hBD-2 binds to the RBD, thereby validating our *in silico* docking and dynamics simulations. Competitive inhibition assays were able to show that hBD-2 reduced RBD:ACE2 binding, possibly by directly binding to the RBD as shown in our biophysical and biochemical assays (Figures 3A–3C). Finally, by incorporating a luciferase reporter expressing CoV-2 spike-dependent lentiviral system (Crawford et al., 2020), we demonstrated that hBD-2 inhibited viral entry into ACE2-expressing HEK 293T cells in a dose-dependent manner, with an IC_{50} of ~2.8 μM. Additionally, hBD-2 begins to show hemolytic activity only at a concentration 25 times greater (70 μM) than our IC_{50} (Koeninger et al., 2020), and shows no signs of cytotoxic effects against various other human cells at over twice our IC_{50} (Herrera et al., 2016; Mi et al., 2018; Sakamoto et al., 2005), suggesting a favorable therapeutic window for hBD-2 against CoV-2 at low micro molar concentrations as shown in this study.

It is important to note that a recent paper by Xu et al., that appeared while our manuscript was under revision, found no blocking activity of hBD-2 in their pseudovirion platform (Xu et al., 2021). While we do not know exactly why our results and theirs differ, we can conjecture that this may have been due to differences in hBD-2 itself, i.e., their hBD-2 was synthesized while ours was recombinantly produced in *E. coli*. While both were presumably one isoform of hBD-2, they may not have been the same isoform. Post-translational modification in folding of the molecule due to varying oxidative conditions that are not controlled in recombinantly generated products can lead to a conformationally different molecule than one that is synthesized (Tokmakov et al., 2012; Wu et al., 2003). Moreover, various isoforms have been reported for beta defensins, and interestingly, have been shown to vary in their biological activity (Wu et al., 2003). Therefore, it would be very interesting to compare the two molecules and determine if indeed conformation plays a role in anti-CoV-2-blocking activity.

Of relevance to our study is the use of smaller mimetics of mouse beta defensin 4 (Zhao et al., 2016), the ortholog of hBD-2, that when administered intra-nasally, rescued 100% of mice from the lethal challenge of human and avian influenza A, SARS-CoV, and MERS-CoV (LeMessurier et al., 2016). The fact that the peptide is endogenous to humans and would not elicit an immunogenic response, gives it a high probability of being safe and a quicker route to human clinical trials. In fact, several AMPs, as well as AMP mimetics, are currently undergoing clinical trials for multiple different diseases (Mookherjee et al., 2020).

Recent biophysical studies using bilayer interferometry predicted a strong binding interaction between LL-37, another human AMP, and the RBD (Wang et al., 2021a). This finding supports the idea that more than one AMP could be utilized, possibly in a "cocktail" to act as a potent blocking agent (Ghosh and Weinberg, 2021). Recent findings also highlight that neuropilin-1 (NRP1), is being utilized by CoV-2 to facilitate entry and infection (Cantuti-Castelvetri et al., 2020; Daly et al., 2020; Li and Buck, 2021)and time will tell if also blocking entry via NRP1 will be required to reduce CoV-2 infection.

Ongoing studies have shown that CoV-2 has developed a number of mutations of which 89 have been associated with the RBD (Chen et al., 2020; Wang et al., 2020b). Furthermore, 52 out of 89 mutations are in the ACE2 receptor-binding motif (RBM), indicating that the virus may be accumulating mutations in that region to increase transmissibility (Li et al., 2020). The flexibility of peptide-based blocking strategies could permit customization to address mutations that could interfere with hBD-2's blocking efficacy (Agarwal and Gabrani, 2020). Additionally, combining hBD-2, or its derivatives, that target the RBD with AMPs (e.g. human defensin 5) that target ACE2 (Wang et al., 2020a) may be efficacious in maintaining therapeutic potential.

The interaction of the RBD with ACE2, and especially with hBD-2, is highly dynamic at the protein interaction molecular level. Although this has not yet been measured in the RBD:ACE2 or RBD:hBD-2 platforms, the entropy of the interaction is likely to be not as unfavorable as seen in complexes where one or both partner proteins have to become significantly rigid. It is now becoming clear that many protein-protein complexes are inherently dynamic (Zhang et al., 2016; Zhang and Buck, 2017), thus minimizing the unfavorable entropy change that would otherwise occur on binding. In fact, this latter indication suggests that peptides, which are initially unstructured in the unbound state could also maintain considerable flexibility in the bound state and may thus be powerful antagonists of the RBD:ACE2 interaction. An alternative would be a mechanism involving entropy-enthalpy compensation, which is observed in many natural systems (Peccati and Jiménez-Osés, 2021). Detailed thermodynamics analyses, both experimental and computational are needed to clarify this point. Nevertheless, our work and that of others suggests that design of AMP-derived peptides and peptide mimetics could be a useful strategy in combating CoV-2 variants (Bakovic et al., 2021; Diamond et al., 2021; Zhang et al., 2021).

We see an AMP strategy as complementary to the new anti-COV-2 vaccines. While they are highly effective, many people are refusing vaccination (Pogue et al., 2020; Schwarzinger et al., 2010) (Fisher et al., 2020; Wang et al., 2021b). Additionally, a significant number either fail to mount effective neutralizing antibodies or high enough titers (Goodwin et al., 2006; Ndifon et al., 2009; Ovsyannikova et al., 2017). Because of the multiple advantages of using small peptides like hBD-2 and their derived smaller mimetics, such as high specificity, low toxicity, lack of immunogenicity, and ease of administration, they possess the potential for both safety and efficacy (Ghosh and Weinberg, 2021) Such molecules could be delivered, in the future, intra-orally and/or intra-nasally as prophylactic aerosols, in early stages of infection, when telltale symptoms appear and in combinatorial therapeutic approaches for more severe situations.

Limitation of the study

A limitation of the study is that the *in vitro* binding experiments were carried out on the RBD, rather than on the entire SARS-Cov-2 spike protein. This was done because the difference in size between the entire S-protein and hBD-2 is so large that the SPR technique would have been rendered insensitive. In addition, docking and MD simulations would have been computationally prohibitive given the resources we have access to. Molecular docking and dynamics calculations are well known to still be limited by the accuracy of the potential function and by the extent of sampling, i.e., number of simulations and their length. Although we cannot be certain that the calculations are highly converged, the results have key predictive value concerning the location and the dynamics of the binding surfaces. A second consideration is that the biophysical affinity measurements by SPR require the labeling of the His-tag with a surface attachment of the RBD via biotin. Although we do not believe this affects the results, as countless control studies on other proteins have shown, we cannot be completely certain. A third consideration is that we showed that hBD-2 inhibits CoV-2 infection by using an experimental system comprising CoV-2 spike protein-expressing pseudovirus particles and HEK293T cells overexpressing ACE2. CoV-2 spike-expressing pseudovirus particles showed only modest infectivity in naturally ACE2-expressing cells such as the human lung cell line A549 and the monkey kidney epithelial cell line Vero, which was not sufficient to derive meaningful conclusions in the competitive inhibition assays. However, because the main objective of this study was to demonstrate the potential for hBD-2 to inhibit viral entry, we believe that the approaches we adopted support the conclusions of this study.

STAR★METHODS

Detailed methods are provided in the online version of this paper and include the following:

- KEY RESOURCES TABLE
- RESOURCE AVAILABILITY

SUPPLEMENTAL INFORMATION

Supplemental information can be found online at https://doi.org/10.1016/j.isci.2022.103856.

ACKNOWLEDGMENTS

LZ: Energy Center of TTU helped support JP; pilot funds (CWRU COVID-19 Patients grant) for AB and JP. PR: We thank Dr. Jesse Bloom, Fred Hutchinson Cancer Center for kindly providing the plasmids to generate Spike pseudovirus and ACE2-expressing HEK 293T cells. PR funded by NIH/NIAID R01AI116730, R21AI144264, NIH/NCI R21CA246194 grants and pilot funding from NORD Family Foundation. MB: We thank Jeannine Muller-Greven for help with the initial MST experiments and Maria Iannucci for the data in Figure S5. MB funded by NIH/NEI R01EY029169 and by a pilot grant from the Department of Physiology and Biophysics of CWRU. AW: Studies herein supported by NIH/NCI R21CA253108, NIH/NIDCR R21DE028416 grants and pilot funds from the Department of Biological Sciences of the School of Dental Medicine, CWRU.

AUTHOR CONTRIBUTIONS

Conceptualization, LZ, SKG, PR, MB, AW. Methodology, LZ, SKG, PR, MB. Investigation, LZ, SCB, JP, AB, SKG, YC, PS, PR. Writing – Original Draft, LZ, SKG, PR, AW. Writing – Review & Editing, SKG, PR, LZ, MB, AW. Visualization, SKG, MB, PR, AW. Supervision, LZ, PR, MB, AW, Project Administration, AW. Funding Acquisition, LZ, MB, PR, AW.

DECLARATION OF INTERESTS

LZ, SKG, PR, MB, and AW are co-inventors in using AMPs, and their derivatives, as anti-coronavirus agents, and have submitted an invention disclosure to Case Western Reserve University. SCB, YC, PS, JP, and AB declare no competing interests.

Received: February 16, 2021
Revised: September 14, 2021
Accepted: January 28, 2022
Published: March 18, 2022

REFERENCES

Agarwal, G., and Gabrani, R. (2020). Antiviral peptides: identification and validation. Int. J. Pept. Res. Ther. 1–20.

Ali, A., and Vijayan, R. (2020). Dynamics of the ACE2-SARS-CoV-2/SARS-CoV spike protein interface reveal unique mechanisms. Sci. Rep. *10*, 14214.

Amaro, R.E., and Mulholland, A.J. (2020). Biomolecular simulations in the time of COVID19, and after. Comput. Sci. Eng. *22*, 30–36.

Bakovic, A., Risner, K., Bhalla, N., Alem, F., Chang, T.L., Weston, W.K., Harness, J.A., and Narayanan, A. (2021). Brilacidin demonstrates inhibition of SARS-CoV-2 in cell culture. Viruses *13*, 271.

Brielle, E.S., Schneidman-Duhovny, D., and Linial, M. (2020). The SARS-CoV-2 exerts a distinctive strategy for interacting with the ACE2 human receptor. Viruses *12*, 497.

Cantuti-Castelvetri, L., Ojha, R., Pedro, L.D., Djannatian, M., Franz, J., Kuivanen, S., van der Meer, F., Kallio, K., Kaya, T., Anastasina, M., et al. (2020). Neuropilin-1 facilitates SARS-CoV-2 cell entry and infectivity. Science *370*, eabd2985.

Chen, J., Wang, R., Wang, M., and Wei, G.W. (2020). Mutations strengthened SARS-CoV-2 infectivity. J. Mol. Biol. *432*, 5212–5226.

Chuang, G.Y., Kozakov, D., Brenke, R., Comeau, S.R., and Vajda, S. (2008). DARS (Decoys as the reference state) potentials for protein-protein docking. Biophys. J. *95*, 4217–4227.

Crawford, K.H.D., Eguia, R., Dingens, A.S., Loes, A.N., Malone, K.D., Wolf, C.R., Chu, H.Y., Tortorici, M.A., Veesler, D., Murphy, M., et al. (2020). Protocol and reagents for pseudotyping lentiviral particles with SARS-CoV-2 spike protein for neutralization assays. Viruses *12*, 513.

Daly, J.L., Simonetti, B., Klein, K., Chen, K.-E., Williamson, M.K., Antón-Plágaro, C., Shoemark, D.K., Simón-Gracia, L., Bauer, M., Hollandi, R., et al. (2020). Neuropilin-1 is a host factor for SARS-CoV-2 infection. Science *370*, eabd3072.

Diamond, G., Molchanova, N., Herlan, C., Fortkort, J.A., Lin, J.S., Figgins, E., Bopp, N., Ryan, L.K., Chung, D., Adcock, R.S., et al. (2021). Potent antiviral activity against HSV-1 and SARS-CoV-2 by antimicrobial peptoids. Pharmaceuticals (Basel) *14*, 304.

Diamond, G., and Ryan, L. (2011). Beta-defensins: what are they really doing in the oral cavity? Oral Dis. *17*, 628–635.

Dominguez, C., Boelens, R., and Bonvin, A.M. (2003). HADDOCK: a protein-protein docking approach based on biochemical or biophysical information. J. Am. Chem. Soc. *125*, 1731–1737.

Fisher, K.A., Bloomstone, S.J., Walder, J., Crawford, S., Fouayzi, H., and Mazor, K.M. (2020). Attitudes toward a potential SARS-CoV-2 vaccine : a survey of U.S. adults. Ann. Intern. Med. *173*, 964–973.

Genheden, S., and Ryde, U. (2015). The MM/PBSA and MM/GBSA methods to estimate ligand-binding affinities. Expert Opin. Drug Discov. *10*, 449–461.

Ghorbani, M., Brooks, B.R., and Klauda, J.B. (2020). Critical sequence hotspots for binding of novel coronavirus to angiotensin converter enzyme as evaluated by molecular simulations. J. Phys. Chem. B *124*, 10034–10047.

Ghosh, S.K., Gerken, T.A., Schneider, K.M., Feng, Z., McCormick, T.S., and Weinberg, A. (2007). Quantification of human beta-defensin-2 and -3 in body fluids: application for studies of innate immunity. Clin. Chem. *53*, 757–765.

Ghosh, S.K., and Weinberg, A. (2021). Ramping up antimicrobial peptides against severe acute respiratory syndrome coronavirus-2. Front. Mol. Biosci. *8*, 620806.

Goodwin, K., Viboud, C., and Simonsen, L. (2006). Antibody response to influenza vaccination in the elderly: a quantitative review. Vaccine *24*, 1159–1169.

Gross, L.Z.F., Sacerdoti, M., Piiper, A., Zeuzem, S., Leroux, A.E., and Biondi, R.M. (2020). ACE2, the receptor that enables infection by SARS-CoV-2: biochemistry, structure, allostery and evaluation of the potential development of ACE2 modulators. ChemMedChem *15*, 1682–1690.

He, J., Tao, H., Yan, Y., Huang, S.Y., and Xiao, Y. (2020). Molecular mechanism of evolution and human infection with SARS-CoV-2. Viruses *12*, 428.

Herrera, R., Morris, M., Rosbe, K., Feng, Z., Weinberg, A., and Tugizov, S. (2016). Human beta-defensins 2 and -3 cointernalize with human immunodeficiency virus via heparan sulfate proteoglycans and reduce infectivity of intracellular virions in tonsil epithelial cells. Virology *487*, 172–187.

Hoover, D.M., Rajashankar, K.R., Blumenthal, R., Puri, A., Oppenheim, J.J., Chertov, O., and Lubkowski, J. (2000). The structure of human beta-defensin-2 shows evidence of higher order oligomerization. J. Biol. Chem. *275*, 32911–32918.

Huang, J., Rauscher, S., Nawrocki, G., Ran, T., Feig, M., de Groot, B.L., Grubmüller, H., and MacKerell, A.D., Jr. (2017). CHARMM36m: an improved force field for folded and intrinsically disordered proteins. Nat. Methods *14*, 71–73.

Humphrey, W., Dalke, A., and Schulten, K. (1996). VMD: visual molecular dynamics. J. Mol. Graph *14*, 27–38.

Idris, M.M., Banu, S., Siva, A.B., and Nagaraj, R. (2020). Downregulation of Defensin genes in SARS-CoV-2 infection. Preprint at. medRxiv. https://doi.org/10.1101/2020.2009.2021.20195537.

Khurshid, Z., Naseem, M., Yahya, I.A.F., Mali, M., Sannam Khan, R., Sahibzada, H.A., Zafar, M.S., Faraz Moin, S., and Khan, E. (2017). Significance and diagnostic role of antimicrobial cathelicidins (LL-37) peptides in oral health. Biomolecules *7*.

Kim, J., Yang, Y.L., Jang, S.H., and Jang, Y.S. (2018). Human β-defensin 2 plays a regulatory role in innate antiviral immunity and is capable of potentiating the induction of antigen-specific immunity. Virol. J. *15*, 124.

Koeninger, L., Armbruster, N.S., Brinch, K.S., Kjaerulf, S., Andersen, B., Langnau, C., Autenrieth, S.E., Schneidawind, D., Stange, E.F., Malek, N.P., et al. (2020). Human β-defensin 2 mediated immune modulation as treatment for experimental colitis. Front. Immunol. *11*, 93.

Kozakov, D., Brenke, R., Comeau, S.R., and Vajda, S. (2006). PIPER: an FFT-based protein docking program with pairwise potentials. Proteins *65*, 392–406.

Kozakov, D., Hall, D.R., Xia, B., Porter, K.A., Padhorny, D., Yueh, C., Beglov, D., and Vajda, S. (2017). The ClusPro web server for protein-protein docking. Nat. Protoc. *12*, 255–278.

Lan, J., Ge, J., Yu, J., Shan, S., Zhou, H., Fan, S., Zhang, Q., Shi, X., Wang, Q., Zhang, L., et al. (2020). Structure of the SARS-CoV-2 spike receptor-binding domain bound to the ACE2 receptor. Nature *581*, 215–220.

Lee, B., and Richards, F.M. (1971). The interpretation of protein structures: estimation of static accessibility. J. Mol. Biol. *55*, 379–400.

Lee, S.H., Kim, J.E., Lim, H.H., Lee, H.M., and Choi, J.O. (2002). Antimicrobial defensin peptides of the human nasal mucosa. Ann. Otol Rhinol Laryngol. *111*, 135–141.

Leikina, E., Delanoe-Ayari, H., Melikov, K., Cho, M.S., Chen, A., Waring, A.J., Wang, W., Xie, Y., Loo, J.A., Lehrer, R.I., et al. (2005). Carbohydrate-binding molecules inhibit viral fusion and entry by crosslinking membrane glycoproteins. Nat. Immunol. *6*, 995–1001.

LeMessurier, K.S., Lin, Y., McCullers, J.A., and Samarasinghe, A.E. (2016). Antimicrobial peptides alter early immune response to influenza A virus infection in C57BL/6 mice. Antivir. Res *133*, 208–217.

Lever, A.M., Strappe, P.M., and Zhao, J. (2004). Lentiviral vectors. J. Biomed. Sci. *11*, 439–449.

Li, Q., Wu, J., Nie, J., Zhang, L., Hao, H., Liu, S., Zhao, C., Zhang, Q., Liu, H., Nie, L., et al. (2020). The impact of mutations in SARS-CoV-2 spike on viral infectivity and antigenicity. Cell *182*, 1284–1294.e9.

Li, Z.L., and Buck, M. (2019). Modified potential functions result in enhanced predictions of a protein complex by all-atom molecular dynamics simulations, confirming a stepwise association process for native protein-protein interactions. J. Chem. Theor. Comput *15*, 4318–4331.

Li, Z.L., and Buck, M. (2021). Neuropilin-1 assists SARS-CoV-2 infection by stimulating the separation of Spike protein S1 and S2. Biophys. J. *120*, 2828–2837.

Mathews, M., Jia, H.P., Guthmiller, J.M., Losh, G., Graham, S., Johnson, G.K., Tack, B.F., and McCray, P.B., Jr. (1999). Production of beta-defensin antimicrobial peptides by the oral mucosa and salivary glands. Infect. Immun. *67*, 2740–2745.

Mi, B., Liu, J., Liu, Y., Hu, L., Liu, Y., Panayi, A.C., Zhou, W., and Liu, G. (2018). The designer antimicrobial peptide A-hBD-2 facilitates skin wound healing by stimulating keratinocyte migration and proliferation. Cell Physiol. Biochem. *51*, 647–663.

Mookherjee, N., Anderson, M.A., Haagsman, H.P., and Davidson, D.J. (2020). Antimicrobial host defence peptides: functions and clinical potential. Nat. Rev. Drug Discov. *19*, 311–332.

Mulder, K.C., Lima, L.A., Miranda, V.J., Dias, S.C., and Franco, O.L. (2013). Current scenario of peptide-based drugs: the key roles of cationic antitumor and antiviral peptides. Front. Microbiol. *4*, 321.

Ndifon, W., Wingreen, N.S., and Levin, S.A. (2009). Differential neutralization efficiency of hemagglutinin epitopes, antibody interference, and the design of influenza vaccines. Proc. Natl. Acad. Sci. U S A *106*, 8701–8706.

Ovsyannikova, I.G., Schaid, D.J., Larrabee, B.R., Haralambieva, I.H., Kennedy, R.B., and Poland, G.A. (2017). A large population-based association study between HLA and KIR genotypes and measles vaccine antibody responses. PLoS One *12*, e0171261.

Peccati, F., and Jiménez-Osés, G. (2021). Enthalpy-entropy compensation in biomolecular recognition: a computational perspective. ACS Omega *6*, 11122–11130. PMID: 34056267; PMCID: PMC8153931. https://doi.org/10.1021/acsomega.1c00485.

Phillips, J.C., Braun, R., Wang, W., Gumbart, J., Tajkhorshid, E., Villa, E., Chipot, C., Skeel, R.D., Kalé, L., and Schulten, K. (2005). Scalable molecular dynamics with NAMD. J. Comput. Chem. *26*, 1781–1802.

Pogue, K., Jensen, J.L., Stancil, C.K., Ferguson, D.G., Hughes, S.J., Mello, E.J., Burgess, R., Berges, B.K., Quaye, A., and Poole, B.D. (2020). Influences on attitudes regarding potential

COVID-19 vaccination in the United States. Vaccines (Basel) *8*, 582.

Porter, K.A., Xia, B., Beglov, D., Bohnuud, T., Alam, N., Schueler-Furman, O., and Kozakov, D. (2017). ClusPro PeptiDock: efficient global docking of peptide recognition motifs using FFT. Bioinformatics *33*, 3299–3301.

Quiñones-Mateu, M.E., Lederman, M.M., Feng, Z., Chakraborty, B., Weber, J., Rangel, H.R., Marotta, M.L., Mirza, M., Jiang, B., Kiser, P., et al. (2003). Human epithelial beta-defensins 2 and 3 inhibit HIV-1 replication. Aids *17*, F39–F48.

Ramakrishnan, P., Wang, W., and Wallach, D. (2004). Receptor-specific signaling for both the alternative and the canonical NF-kappaB activation pathways by NF-kappaB-inducing kinase. Immunity *21*, 477–489.

Ryan, L.K., Dai, J., Yin, Z., Megjugorac, N., Uhlhorn, V., Yim, S., Schwartz, K.D., Abrahams, J.M., Diamond, G., and Fitzgerald-Bocarsly, P. (2011). Modulation of human beta-defensin-1 (hBD-1) in plasmacytoid dendritic cells (PDC), monocytes, and epithelial cells by influenza virus, Herpes simplex virus, and Sendai virus and its possible role in innate immunity. J. Leukoc. Biol. *90*, 343–356.

Sakamoto, N., Mukae, H., Fujii, T., Ishii, H., Yoshioka, S., Kakugawa, T., Sugiyama, K., Mizuta, Y., Kadota, J., Nakazato, M., et al. (2005). Differential effects of alpha- and beta-defensin on cytokine production by cultured human bronchial epithelial cells. Am. J. Physiol. Lung Cell Mol. Physiol. *288*, L508–L513.

Sawai, M.V., Jia, H.P., Liu, L., Aseyev, V., Wiencek, J.M., McCray, P.B., Jr., Ganz, T., Kearney, W.R., and Tack, B.F. (2001). The NMR structure of human beta-defensin-2 reveals a novel alpha-helical segment. Biochemistry *40*, 3810–3816.

Schwarzinger, M., Flicoteaux, R., Cortarenoda, S., Obadia, Y., and Moatti, J.P. (2010). Low acceptability of A/H1N1 pandemic vaccination in French adult population: did public health policy fuel public dissonance? PLoS One *5*, e10199.

Singh, P.K., Jia, H.P., Wiles, K., Hesselberth, J., Liu, L., Conway, B.A., Greenberg, E.P., Valore, E.V., Welsh, M.J., Ganz, T., et al. (1998). Production of beta-defensins by human airway epithelia. Proc. Natl. Acad. Sci. U S A *95*, 14961–14966.

Siu, Y.L., Teoh, K.T., Lo, J., Chan, C.M., Kien, F., Escriou, N., Tsao, S.W., Nicholls, J.M., Altmeyer, R., Peiris, J.S., et al. (2008). The M, E, and N structural proteins of the severe acute respiratory syndrome coronavirus are required for efficient assembly, trafficking, and release of virus-like particles. J. Virol. *82*, 11318–11330.

Spinello, A., Saltalamacchia, A., and Magistrato, A. (2020). Is the rigidity of SARS-CoV-2 spike receptor-binding motif the hallmark for its enhanced infectivity? Insights from all-atom simulations. J. Phys. Chem. Lett. *11*, 4785–4790.

Tai, W., He, L., Zhang, X., Pu, J., Voronin, D., Jiang, S., Zhou, Y., and Du, L. (2020). Characterization of the receptor-binding domain (RBD) of 2019 novel coronavirus: implication for development of RBD protein as a viral attachment inhibitor and vaccine. Cell Mol. Immunol. *17*, 613–620.

Tanner, D.E., Chan, K.Y., Phillips, J.C., and Schulten, K. (2011). Parallel generalized born implicit solvent calculations with NAMD. J. Chem. Theor. Comput. *7*, 3635–3642.

Tokmakov, A.A., Kurotani, A., Takagi, T., Toyama, M., Shirouzu, M., Fukami, Y., and Yokoyama, S. (2012). Multiple post-translational modifications affect heterologous protein synthesis. J. Biol. Chem. *287*, 27106–27116.

Vajda, S., Yueh, C., Beglov, D., Bohnuud, T., Mottarella, S.E., Xia, B., Hall, D.R., and Kozakov, D. (2017). New additions to the ClusPro server motivated by CAPRI. Proteins *85*, 435–444.

van Zundert, G.C.P., Rodrigues, J., Trellet, M., Schmitz, C., Kastritis, P.L., Karaca, E., Melquiond, A.S.J., van Dijk, M., de Vries, S.J., and Bonvin, A. (2016). The HADDOCK2.2 web server: user-friendly integrative modeling of biomolecular complexes. J. Mol. Biol. *428*, 720–725.

Wang, C., Wang, S., Li, D., Chen, P., Han, S., Zhao, G., Chen, Y., Zhao, J., Xiong, J., Qiu, J., et al. (2021a). Human cathelicidin inhibits SARS-CoV-2 infection: killing two birds with one stone. ACS Infect. Dis. *7*, 1545–1554.

Wang, C., Wang, S., Li, D., Wei, D.Q., Zhao, J., and Wang, J. (2020a). Human intestinal defensin 5 inhibits SARS-CoV-2 invasion by cloaking ACE2. Gastroenterology *159*, 1145–1147.e4.

Wang, J., Feng, Y., Hou, Z., Lu, Y., Chen, H., Ouyang, L., Wang, N., Fu, H., Wang, S., Kan, X., et al. (2021b). Willingness to receive SARS-CoV-2 vaccine among healthcare workers in public institutions of Zhejiang Province, China. Hum. Vaccin. Immunother. *17*, 2926–2933.

Wang, R., Hozumi, Y., Yin, C., and Wei, G.W. (2020b). Decoding SARS-CoV-2 transmission and evolution and ramifications for COVID-19 diagnosis, vaccine, and medicine. J. Chem. Inf. Model. *60*, 5853–5865.

Wrapp, D., Wang, N., Corbett, K.S., Goldsmith, J.A., Hsieh, C.L., Abiona, O., Graham, B.S., and McLellan, J.S. (2020). Cryo-EM structure of the 2019-nCoV spike in the prefusion conformation. Science *367*, 1260–1263.

Wu, Z., Hoover, D.M., Yang, D., Boulègue, C., Santamaria, F., Oppenheim, J.J., Lubkowski, J., and Lu, W. (2003). Engineering disulfide bridges to dissect antimicrobial and chemotactic activities of human beta-defensin 3. Proc. Natl. Acad. Sci. U S A *100*, 8880–8885.

Xu, C., Wang, A., Marin, M., Honnen, W., Ramasamy, S., Porter, E., Subbian, S., Pinter, A., Melikyan, G.B., Lu, W., et al. (2021). Human defensins inhibit SARS-CoV-2 infection by blocking viral entry. Viruses *13*, 1246.

Yoshimoto, F.K. (2020). The proteins of severe acute respiratory syndrome coronavirus-2 (SARS CoV-2 or n-COV19), the cause of COVID-19. Protein J. *39*, 198–216.

Zhang, L., Borthakur, S., and Buck, M. (2016). Dissociation of a dynamic protein complex studied by all-atom molecular simulations. Biophys. J. *110*, 877–886.

Zhang, L., and Buck, M. (2017). Molecular dynamics simulations reveal isoform specific contact dynamics between the plexin Rho GTPase binding domain (RBD) and small Rho GTPases Rac1 and Rnd1. J. Phys. Chem. B *121*, 1485–1498.

Zhang, R., Jiang, X., Qiao, J., Wang, Z., Tong, A., Yang, J., Yang, S., and Yang, L. (2021). Antimicrobial peptide DP7 with potential activity against SARS coronavirus infections. Signal. Transduct. Target. Ther. *6*, 140.

Zhao, H., Zhou, J., Zhang, K., Chu, H., Liu, D., Poon, V.K., Chan, C.C., Leung, H.C., Fai, N., Lin, Y.P., et al. (2016). A novel peptide with potent and broad-spectrum antiviral activities against multiple respiratory viruses. Sci. Rep. *6*, 22008.

STAR★METHODS

KEY RESOURCES TABLE

REAGENT or RESOURCE	SOURCE	IDENTIFIER
Antibodies		
Anti-Human BD-2	Peprotech, NJ	Cat#5 500-p161G; RRID:AB_147819
Biotinylated Anti-Human BD-2	Peprotech, NJ	Cat#500-P161GBT; RRID:AB_147820
ACE2 Rabbit Ab	Cell signaling	Cat#4355S; RRID:AB_2797606
Monoclonal Anti-HIS tag antibody produced in mouse	Sigma Aldrich	Cat#SAB1305538; RRID:AB_2687993
Anti-Goat IgG HRP conjugate	Santa Cruz biotechnology	Cat#SC-2020; RRID:AB_631728
Anti-Mouse IgG HRP conjugate	Cell signaling	Cat#7076s; RRID:AB_330924
Anti-Rabbit IgG HRP conjugate	Cell signaling	Cat#7074s; RRID:AB_2099233
Chemicals, peptides, and recombinant proteins		
Human Beta Defensin-2 (hBD-2)	Peprotech, NJ	Cat#:300-49
LL37	TOCRIS Bioscience	Cat#5213
Recombinant SARS COV-2 spike protein (RBD HIS tag)	Sino biological Inc	Cat#40592-V088 LC1MC 1106
Ni-NTA Agarose	QIAGEN	Cat#30210
Polybrene	Millipore sigma	Cat#TR-1003-G
SARS-CoV-2 (2019-nCoV) Spike RBD-His Recombinant Protein, Biotinylated	Sino Biological Inc	Cat#40592-V08H-B
His-Tag Labeling Kit RED-tris-NTA 2nd Generation	NanoTemper	Cat#MO-L018
Critical commercial assays		
Dual-Luciferase reporter assay system	Promega	Cat#E1960
Experimental models: Cell lines		
HEK293T-ACE2 cells	Gift (Dr. Jesse D Bloom)	Crawford et al. (2020)
Recombinant DNA		
SARS-CoV2 Spike-ALAYT, pHAGE-CMV-Luc2-IRES-Zsgreen, HDM-HgPM2, HDM-tat1b, PRC-CMV-Rev1b plasmids	Gift (Dr. Jesse D Bloom)	Crawford et al. (2020)
SARS-CoV-2 (2019-nCoV) Spike (RBD) ORF mammalian expression plasmid, N-His tag	Sino biological Inc	#VG40592-NH
Software and algorithms		
Prism software	GraphPad	V9.1.0
BIAevaluation Software	GE Healthcare/Cytiva	GE Healthcare
Origin	OriginLab	OriginLab
MO.Affinity Analysis	NanoTemper	v2.2.6
NAMD for simulation	UIUC, Free for academic	Edition 2.12
VMD for trajectory analysis	UIUC, Free for academic	Edition 1.9.3
Other		
Sensor Chip SA	Cytiva	Cat#29104992
Monolith Premium Capillaries	NanoTemper	Cat#CMO-K025
S-RBD-coated Microplate	RayBiotech	Cat#CoV-SACE2
Streptavidin-HRP	R&D Systems	Cat#DY998
Quantikine ELISA Wash Buffer 1	R&D Systems	Cat# WA126

RESOURCE AVAILABILITY

Lead contact

Further information and requests for resources and reagents should be directed to, and will be fulfilled by, the lead contact, Aaron Weinberg (axw47@case.edu).

Materials availability

This study did not generate new unique reagents.

Data and code availability

The data reported in this paper will be shared upon request [Lead contact: Aaron Weinberg (axw47@case.edu)]. This paper does not report original code. Any additional information required to reanalyze the data reported in this paper is available from the lead contact upon request.

EXPERIMENTAL MODEL AND SUBJECT DETAILS

Cells

HEK 293T and HEK 293T cells stably expressing ACE2 receptor (ACE2 HEK293T) were cultured in DMEM media containing 10% heat inactivated FBS, 100 U/ml penicillin/streptomycin and 4 mM L-Glutamine.

Plasmids

pHAGE-CMV-Luc2-IRES-ZSgreen-W, HDM-HgPM2, HDM-tat1b, pRC-CMV-Rev1b, and SARS-CoV-2 Spike-ALAYT plasmids (Crawford et al., 2020). HIS tagged RBD was expressed from a pcDNA3 vector with leader sequence and leucine zipper (Ramakrishnan et al., 2004).

Structure information

The structure of human beta defensin 2 (hBD-2) in the monomer and dimer form is available in the PDB:1FD3 (Hoover et al., 2000). The hBD-2 sequence is 41 residues long: GIGDPVTCLKSGAICHPVFCPR-RYKQIGTCGLPGTKCCKKP. The five residues in bold were found to form hydrogen bonds with the RBD during the simulations (see below/main paper). The structure of the RBD domain of the Spike protein is also available in complex with ACE2 at 2.45 Å resolution in the PDB:6M0J (Lan et al., 2020) and was used in reference simulations.

METHOD DETAILS

Docking and all-atom simulations

Two kinds of docking programs were applied; CLUSPRO (Kozakov et al., 2006, 2017; Porter et al., 2017; Vajda et al., 2017) and HADDOCK (Dominguez et al., 2003; van Zundert et al., 2016). The x-ray structures of hBD-2 and of the SARS-CoV-2 S-protein RBD were uploaded to the CLUSPRO docking webserver without additional preparation. The hBD-2 : RBD docked structures were clustered, and the best of these clustered structures, in terms of the population of clusters, involved sites on the side of the RBD which are utilized in binding ACE2. The best structure was selected based on the docking programs' score. The CLUSPRO method is based on a Fast Fourier Transform correlation approach, which makes it feasible to generate and evaluate billions of docked conformations by simple scoring functions as shown in Equation (1). It is a multistage protocol: rigid body docking using PIPER (Kozakov et al., 2006), an energy based filtering (using interaction energy calculated with Equation 1), ranking the retained structures based on clustering properties, and finally, the refinement of a limited number of structures by energy minimization.

$$\text{Interaction energy } E = 0.40E_{rep} - 0.40E_{att} + 600E_{elec} + 1.00E_{DARS} \quad \text{(Equation 1)}$$

Here, E_{rep} and E_{att} are contributions of the van der Waals interaction energy, and E_{elec} is an electrostatic energy term. E_{DARS} is a pairwise structure-based potential constructed by the Decoys as the Reference State (DARS) method (Chuang et al., 2008). Since an entropic term was not included in CLUSPRO docking, the energy result should not be used to rank clusters and the population of clusters was used to rank them.

The population of clusters was applied to rank the clusters. In our simulations, the RBD:hBD-2 complex structure from the top cluster was taken and continued with all-atom molecular dynamics simulations.

By contrast to CLUSPRO, the docking HADDOCK had to be more selective and since the binding interface between the ACE2 receptor and RBD are known, residues from 400 to 520 on the RBD were selected as the target binding sites, while the entire hBD-2 peptide taken as a potential binding site. Default values for all other parameters were applied. After that, the best 5 structures, by HADDOCK scoring, were selected.

Based on the best 6 (including above 5 from HADDOCK and 1 from CLUSPRO docking) structures predicted above, all-atom molecular dynamics simulations were set up using the CHARMM36m (Huang et al., 2017) forcefield and VMD program (Humphrey et al., 1996). One of the deprotonated states of histidine was used (denoted HSD), and the native disulfide bonding in the hBD-2 was set up. After solvating the protein with an equilibrated box of TIP3P water molecules, the closest distance between atoms on the proteins and the edge of simulation box is 12 Å. The equivalent of 0.15 M in Na^+ and Cl^- ions was added into the box plus several ions to neutralize the net charge of the system. The simulation temperature was kept at 310 K and pressure at 1 atm, using standard thermo- and barostats. After a brief energy minimization using the conjugate gradient and line search algorithm, 4 ps of dynamics was run at 50 K, and then the system was brought up to 310 K over an equilibration period of 1 ns using NAMD program version 2.12 (Phillips et al., 2005). This was followed by trajectories that continued for up to 200 or 500 ns at 1 atm and 310 K using the NPT ensemble. The trajectory shown in Figures 1B and 2 was started from the best CLUSPRO docked structure. The final structure was restarted with three different random seeds (velocity assignments) for another 500 ns, denoted C1, C2 and C3 in Figure S2.

As a comparison, we also simulated the RBD bound with ACE2 using the structures from (Lan et al., 2020) and the same method as above. HBD-2 can also form a non-covalent dimer at high concentration in solution (Hoover et al., 2000) (PDB:1FD3). The initial bound structure of the hBD-2 dimer with the RBD was predicted using targeted HADDOCK docking. The best structure predicted was used in all-atom MD simulations as detailed above.

The simulation systems, set up, the number of atoms and box size information are shown in Table S1. To analyze the trajectories, the Root Mean Square Deviation (RMSD) and Fluctuations (RMSF) of the proteins were calculated using the VMD program and an in-house analysis script based on the coordinates of the backbone Ca atoms after aligning the trajectories respectively, to the original crystal structure of the RBD, hBD-2, and to the initial complex structure of the RBD and hBD-2 predicted from docking. The buried surface area (BSA) for the complex was calculated in two steps using the VMD program and a script using the Richards and Lee method with the water probe size of 1.4 Å (Lee and Richards, 1971). First, the total solvent accessible surface area of the complex ($ASA_{complex}$) was calculated based on the complex's trajectory. Second, the accessible surface area of each protein in the complex (ASA_{rbd}, ASA_{hbd2}) was calculated for each protein individually. Then, the buried surface area, BSA is calculated using Equation (2):

$$BSA = 0.5*(ASA_{rbd} + ASA_{hbd2} - ASA_{complex}) \quad \text{(Equation 2)}$$

The number of hydrogen bonds between the RBD and ACE2 or the RBD and hBD-2 were calculated using the VMD program with the heavy atom distance cutoff of 3.0 Å and the angle cutoff of 20 degrees deviation from H-bond linearity. The time a particular H-bond is formed over the course of the simulation is monitored and is expressed as % occupancy. In order to find out the residues on the binding interface, the closest distance between every residue atom (including hydrogen) between the RBD and hBD-2 was calculated and averaged over the trajectory run. The average distances between each residue on RBD and on hBD-2 are shaded by proximity on a red to white color-scale and were used to build the distance maps. Due to the caveats associated with calculations of free energy estimations from trajectories such as the ones run for this study, we carried out the binding interaction energy calculation for RBD binding with ACE2 and hBD-2 monomer/dimer, respectively, using the popular MM-GBSA method (Genheden and Ryde, 2015). This total pairwise interaction energy was calculated over the entire trajectory by NAMD energy plugin of the VMD and results are shown in Table S1, (Humphrey et al., 1996). This interaction energy (E_binding) is calculated using Equation (3):

$$E\_binding = \langle E\_complex \rangle - \langle E\_protein \rangle - \langle E\_ligand \rangle \quad \text{(Equation 3)}$$

E_complex is the potential energy of protein-ligand complex, E_protein is the potential energy of protein, and E_ligand is the potential energy of ligand. < > is the ensemble average over simulation time.

In the MM-GBSA method, the solvent effect was counted using the generalized Born implicit solvent model (GBIS) (Tanner et al., 2011).(He et al., 2020)

Measuring RBD:ACE2 association *in vitro*

Untagged recombinant hBD-2 and C-terminally His-tagged biotinylated recombinant RBD were purchased from Peprotech, Inc. and SinoBiological Inc., respectively. Earlier experiments with His-tagged, but not biotinylated rRBDs indicated a slower second kinetic phase in SPR, which did not show saturation behavior (possibly aggregation of the rhBD-2) and could not be used for fitting. Using, surface plasmon resonance (SPR), the measurements were carried out at 25ºC using a BIAcore T200 (Cytiva, formerly GE Healthcare) in PBSP buffer with 0.3 mg/mL of BSA. Biotinylated RBD was captured to an S series SA sensor chip (Cytiva) at a density of 2600RU. Samples of the rhBD-2 at 90.23, 180.47, 360.94, 721.88, 1443.75, 2887.5, 5775, 11550, and 23100 nM were injected at 30 μL/min over the rRBD. Data were analyzed using the BIAevaluation software using two-state binding model and redrawn by Origin software. A second experiment was carried out a day later and the two Kd's were averaged.

ELISA based assay

100 μl of rhBD-2 (Peprotech, Inc.) (concentration ranges 0.00024 to 2 μM) in assay diluent buffer 2 (R&D system) containing 1% BSA in PBS, were incubated in an RBD coated plate (Ray biotech, Inc.) at 4°C for 18 hrs. To test specificity of hBD-2 binding to RBD, we coated the microplate with LL37 (2ug/ml) as a negative control. Plates were then washed 4 times with 300 μl of 1X Quantikine ELISA wash buffer (R&D Systems, Inc.) followed by incubation with 100 μl of biotinylated anti-hBD-2 (Peprotech, Inc.) [0.1 μg/ml] for 1 hr. Plates were then washed again as stated above, incubated with 100 μl of Streptavidin-HRP (R&D system, Inc.) for 20 minutes. Signal was developed using TMB substrate and measured at 450 nm using a microplate reader.

Ni-NTA precipitation, immunoprecipitation and western blotting

To study the interaction between recombinant hBD-2 (Peprotech, Inc.) and recombinant HIS-tagged-RBD (Sino Biologicals, Inc.), rhBD-2 (1.75 μM) and rRBD (0.19 μM) were preincubated in a buffer containing 20 mM HEPES, 5 mM $MgCl_2$ and 150 mM NaCl (solution A; 400ul) at room temperature for 1 hour. The binding reaction was then mixed with 1:1 volume of buffer containing 20 mM HEPES, 5 mM $MgCl_2$, 150 mM NaCl, 0.5 mM DTT, 1% triton X 100 and 1mm EDTA (solution B) and incubated with Ni-NTA agarose resin beads (25 μl; Qiagen) overnight at 4°C. Standard IP protocols call for adding low amounts of DTT and triton X 100 to reduce possible non-specific cysteine reactions and non-specific sticking of reagents in the tube as well as to decrease protein degradation (possibly by decreasing protease activity). After overnight incubation, Ni-NTA beads were collected by centrifugation at 1000 rpm for 1 min and washed thrice with binding buffer. Beads were boiled with 30 μl of Laemmli sample buffer and were analyzed by Western blotting (WB). Briefly, samples were separated on 20% SDS-Polyacrylamide gels and proteins were then transferred to nitrocellulose membrane (0.2 μm pore size) at 70V for 40 min in cold. Membranes were blocked with 5% milk in TBST and then probed with goat anti-human BD2 antibody (0.2 μg/ml; Peprotech), followed by secondary antibody (1:5000) at room temperature, and visualized by enhanced chemiluminescence. To study the ability of hBD2 to compete with RBD binding to ACE2, ACE2 HEK 293T cells were seeded in 6 cm plates. At 50% confluency, media was replaced with conditioned media from HEK 293T cells transfected with secreted HIS-RBD plasmid or control media in the presence or absence of rhBD-2 (0.7-2.1 μM) and incubated at 37°C for 30 min. Cells were washed and collected in PBS-EDTA solution and then lysed in Triton lysis buffer. Lysates were centrifuged at 12000 g for 10 min at 4°C, and immunoprecipitated using Ni-NTA beads for 2 hours at 4°C. Beads were collected, washed, and boiled with Laemmli sample buffer and analyzed by Western blotting.

CoV-2 spike-pseudotyped luciferase assay

Pseudotyped SARS-CoV-2 spike virus was generated and the luciferase assay was carried (Crawford et al., 2020). HEK 293T cells were transfected with luciferase-IRES-Zs Green, HDM-HgPM2, HDM-tat1b, PRC-CMV-Rev1b, and SARS-CoV-2 Spike-ALAYT plasmids (Crawford et al., 2020). Culture supernatants were harvested 48 hours after transfection and used to infect ACE2 HEK293T cells. To perform *in-vitro* infections, cells were incubated for 48 h with different dilutions of spike or VSVG- pseudotyped virus in culture media to arrive at similar RLUs. Cells were lysed and luminescence was measured using the luciferase assay system following the manufacturer's instructions (Promega, Inc.) in Spectramax i3 microplate detection platform (Molecular Devices, Inc.). Based on the preliminary experiments, 1:0 dilution for spike-pseudotyped virus

and 1:1000 dilution for VSVG- pseudotyped virus, which exhibits similar RLUs, was selected for further experiments. To study the effect of hBD-2 on spike pseudotyped virus entry, rhBD-2 and pseudovirus with similar RLUs were added to cells simultaneously. ACE2 expressing HEK293T cells were co-incubated with 100 μl of spike-pseudotyped virus media (1:0 diluted in culture media) or VSVG-pseudotyped virus media (1:1000 diluted in culture media) and varying concentration of rhBD-2 (0-25.6 μM) with the final assay volume of 200 μl for 48 hours. Cells were lysed and luminescence was measured.

QUANTIFICATION AND STATISTICAL ANALYSIS

Values are expressed as mean ± SEM and evaluated statistically using Graphpad Prism. Significance between the groups was analyzed by performing one-way ANOVA with Tukey post-t-test. $P < 0.05$ was considered statistically significant. ***$p < 0.001$, **$p < 0.01$, *$p < 0.05$, and ns (non-significant).